For a homogeneous sphere of radius a, $r_g = \frac{5}{3}a$.

From equation (2.28) the gravitational potential of a homogeneous sphere of radius a is

$$\Phi(r) = \begin{cases} -2\pi G\rho(a^2 - \frac{1}{3}r^2) & (r < a), \\ -\dfrac{4\pi G\rho a^3}{3r} & (r > a). \end{cases} \tag{2.43}$$

(c) Plummer model We might expect that in many spherical systems the density is roughly constant near the center, and falls to zero at large radii. The potential of a system of this type would be proportional to $r^2 +$ *constant* at small radii and to r^{-1} at large radii. A simple potential with these properties is the **Plummer model**

$$\Phi = -\frac{GM}{\sqrt{r^2 + b^2}}. \tag{2.44a}$$

The linear scale of the system that generates this potential is set by the **Plummer scale length** b, while M is the system's total mass.

From equation (B.53) for ∇^2 in spherical polar coordinates we have

$$\nabla^2\Phi = \frac{1}{r^2}\frac{\mathrm{d}}{\mathrm{d}r}\left(r^2\frac{\mathrm{d}\Phi}{\mathrm{d}r}\right) = \frac{3GMb^2}{(r^2 + b^2)^{5/2}}. \tag{2.45}$$

Thus from Poisson's equation (2.10) we have that the density corresponding to the potential (2.44a) is

$$\rho(r) = \frac{3M}{4\pi b^3}\left(1 + \frac{r^2}{b^2}\right)^{-5/2}. \tag{2.44b}$$

The potential energy of a Plummer model is

$$W = -\frac{3\pi GM^2}{32b}. \tag{2.46}$$

Plummer (1911) used the potential-density pair that is described by equations (2.44) to fit observations of globular clusters. We shall encounter it again in §4.3.3a as a member of the family of stellar systems known as polytropes.

(d) Isochrone potential The position of a star orbiting in a Plummer potential cannot be given in terms of elementary functions. However, in Chapter 3 we shall see that all orbits are analytic in the **isochrone potential**

$$\Phi(r) = -\frac{GM}{b + \sqrt{b^2 + r^2}}, \tag{2.47}$$

for then equations (3.68a) become

$$\ddot{x} = -\kappa^2 x, \tag{3.78a}$$

$$\ddot{z} = -\nu^2 z. \tag{3.78b}$$

According to these equations, x and z evolve like the displacements of two harmonic oscillators, with frequencies κ and ν, respectively. The two frequencies κ and ν are called the **epicycle** or **radial frequency** and the **vertical frequency**. If we substitute from equation (3.68b) for $\Phi_{\rm eff}$ we obtain[3]

$$\kappa^2(R_{\rm g}) = \left(\frac{\partial^2\Phi}{\partial R^2}\right)_{(R_{\rm g},0)} + \frac{3L_z^2}{R_{\rm g}^4} = \left(\frac{\partial^2\Phi}{\partial R^2}\right)_{(R_{\rm g},0)} + \frac{3}{R_{\rm g}}\left(\frac{\partial\Phi}{\partial R}\right)_{(R_{\rm g},0)}, \tag{3.79a}$$

$$\nu^2(R_{\rm g}) = \left(\frac{\partial^2\Phi}{\partial z^2}\right)_{(R_{\rm g},0)}. \tag{3.79b}$$

Since the circular frequency is given by

$$\Omega^2(R) = \frac{1}{R}\left(\frac{\partial\Phi}{\partial R}\right)_{(R,0)} = \frac{L_z^2}{R^4}, \tag{3.79c}$$

equation (3.79a) may be written

$$\kappa^2(R_{\rm g}) = \left(R\frac{{\rm d}\Omega^2}{{\rm d}R} + 4\Omega^2\right)_{R_{\rm g}}. \tag{3.80}$$

Note that the radial and azimuthal periods (eqs. 3.17 and 3.19) are simply

$$T_r = \frac{2\pi}{\kappa} \quad ; \quad T_\psi = \frac{2\pi}{\Omega}. \tag{3.81}$$

Very near the center of a galaxy, where the circular speed rises approximately linearly with radius, Ω is nearly constant and $\kappa \simeq 2\Omega$. Elsewhere Ω declines with radius, though rarely faster than the Kepler falloff, $\Omega \propto R^{-3/2}$, which yields $\kappa = \Omega$. Thus, in general,

$$\Omega \lesssim \kappa \lesssim 2\Omega. \tag{3.82}$$

Using equations (3.19) and (3.81), it is easy to show that this range is consistent with the range of $\Delta\psi$ given by equation (3.41) for the isochrone potential.

[3] The formula for the ratio κ^2/Ω^2 from equations (3.79) was already known to Newton; see Proposition 45 of his *Principia*.

or

$$q_\rho^2 \simeq q_\Phi^4 \left(2 - \frac{1}{q_\Phi^2}\right) \quad (r \gg R_c). \tag{2.72b}$$

Outside the core, the flattening $1 - q_\Phi$ of the potential is only about a third that of the density distribution: $1 - q_\Phi \simeq \frac{1}{3}(1 - q_\rho)$. The density ρ_L becomes negative on the z axis when $q_\Phi < 1/\sqrt{2} = 0.707$.

2.3.3 Poisson's equation in very flattened systems

In any axisymmetric system with density $\rho(R, z)$, Poisson's equation can be written (eq. B.52)

$$\frac{\partial^2 \Phi}{\partial z^2} = 4\pi G\rho(R, z) + \frac{1}{R}\frac{\partial}{\partial R}(RF_R), \tag{2.73}$$

where $F_R = -\partial\Phi/\partial R$ is the radial force. Now consider, for example, the Miyamoto–Nagai potential-density pair given by equations (2.69). As the parameter $b \to 0$, the density distribution becomes more and more flattened, and at fixed R the density in the plane $z = 0$ becomes larger and larger as b^{-1}. However, the radial force F_R remains well behaved as $b \to 0$; indeed, in the limit $b = 0$, $F_R = -\partial\Phi_K/\partial R$, where $\Phi_K(R, z)$ is simply the Kuzmin potential (2.68a). Thus, near $z = 0$ the first term on the right side of equation (2.73) becomes very large compared to the second, and Poisson's equation simplifies to the form

$$\frac{\partial^2 \Phi(R, z)}{\partial z^2} = 4\pi G\rho(R, z). \tag{2.74}$$

This result applies to almost any thin disk system. It implies that the vertical variation of the potential at a given radius R depends only on the density distribution at that radius. Effectively, this means that the solution of Poisson's equation in a thin disk can be decomposed into two steps: (i) Approximate the thin disk as a surface density layer of zero thickness and determine the potential in the plane of the disk $\Phi(R, 0)$ using the models of this section or the more general techniques of §2.6. (ii) At each radius R solve equation (2.74) to find the vertical variation of $\Phi(R, z)$.

Thus we have

$$\Phi(R, z) = \Phi(R, 0) + \Phi_z(R, z) \tag{2.75a}$$

where

$$\Phi_z(R, z) \equiv 4\pi G \int_0^z \mathrm{d}z' \int_0^{z'} \mathrm{d}z'' \rho(R, z'') + a(R)z. \tag{2.75b}$$

The constant of integration, a, is zero if the disk is symmetric around the equatorial plane.

If we evaluate the coefficient of the small quantity x at R_0 rather than R_g, we introduce an additional error in $v_\phi(R_0)$ which is of order x^2 and therefore negligible. Making this approximation we find

$$v_\phi(R_0) - v_c(R_0) \simeq -x\left(2\Omega + R\frac{d\Omega}{dR}\right)_{R_0}. \tag{3.96c}$$

Finally using equations (3.83) to introduce Oort's constants, we obtain

$$v_\phi(R_0) - v_c(R_0) \simeq 2Bx = \frac{\kappa}{\gamma}x = \frac{\kappa}{\gamma}X\cos(\kappa t + \alpha). \tag{3.97}$$

Averaging over the phases α of stars near the Sun, we find

$$\overline{[v_\phi - v_c(R_0)]^2} = \frac{\kappa^2 X^2}{2\gamma^2} = 2B^2X^2. \tag{3.98}$$

Similarly, we may neglect the dependence of κ on R_g to obtain with equation (3.84)

$$\overline{v_R^2} = \tfrac{1}{2}\kappa^2 X^2 = -2B(A-B)X^2. \tag{3.99}$$

Taking the ratio of the last two equations we have

$$\frac{\overline{[v_\phi - v_c(R_0)]^2}}{\overline{v_R^2}} \simeq \frac{-B}{A-B} = -\frac{B}{\Omega_0} = \frac{\kappa_0^2}{4\Omega_0^2} = \gamma^{-2} \simeq 0.46. \tag{3.100}$$

In §4.4.3 we shall re-derive this equation from a rather different point of view and compare its predictions with observational data.

Note that the ratio in equation (3.100) is the *inverse* of the ratio of the mean-square azimuthal and radial velocities relative to the guiding center: by (3.95)

$$\frac{\overline{\dot{y}^2}}{\overline{\dot{x}^2}} = \frac{\frac{1}{2}(\kappa Y)^2}{\frac{1}{2}(\kappa X)^2} = \gamma^2. \tag{3.101}$$

This counter-intuitive result arises because one measure of the RMS tangential velocity (eq. 3.101) is taken with respect to the guiding center of a single star, while the other (eq. 3.100) is taken with respect to the circular speed at the star's instantaneous radius.

This analysis also leads to an alternative expression for the integral of motion H_R defined in equation (3.86). Eliminating x using equation (3.97), we have

$$H_R = \tfrac{1}{2}\dot{x}^2 + \tfrac{1}{2}\gamma^2[v_\phi(R_0) - v_c(R_0)]^2. \tag{3.102}$$

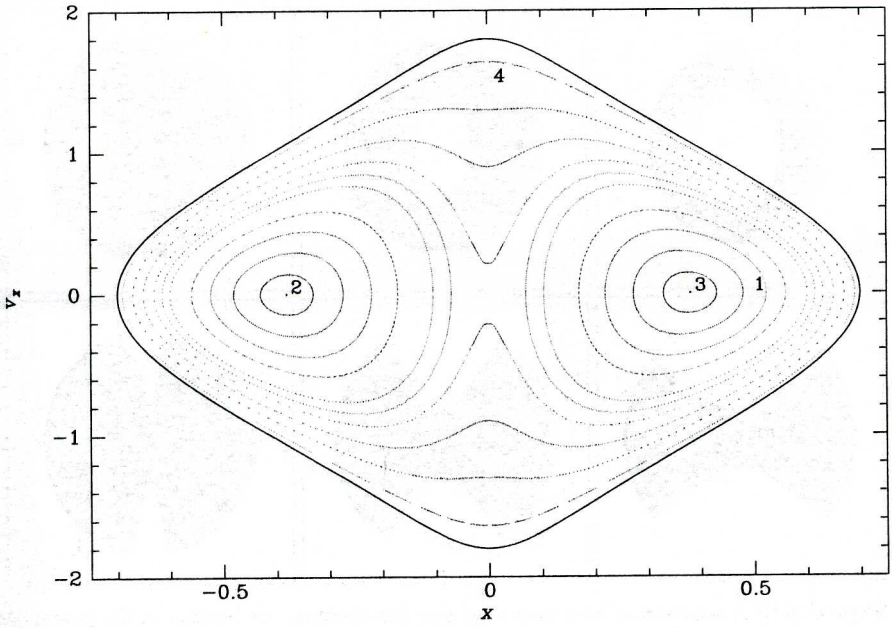

Figure 3.9 The $(x, \dot{x})$ surface of section formed by orbits in $\Phi_{\rm L}$ of the same energy as the orbits depicted in Figure 3.8. The isopotential surface of this energy cuts the long axis at $x = 0.7$. The curves marked 4 and 1 correspond to the box and loop orbits shown in the top and bottom panels of Figure 3.8.

the thickness of the rosette formed by an orbit of given energy in a planar axisymmetric potential depends on its angular momentum. This analogy suggests that stars on loop orbits in $\Phi_{\rm L}$ may respect an integral that is some sort of generalization of the angular momentum p_ϕ.

We may investigate these orbits further by generating a surface of section. Figure 3.9 is the surface of section $y = 0$, $\dot{y} > 0$ generated by orbits in $\Phi_{\rm L}$ of the same energy as the orbits shown in Figure 3.8. The boundary curve in this figure arises from the energy constraint

$$\tfrac{1}{2}\dot{x}^2 + \Phi_L(x,0) \leq \tfrac{1}{2}(\dot{x}^2 + \dot{y}^2) + \Phi_L(x,0) = H_{y=0}. \qquad (3.106)$$

Each closed curve in this figure corresponds to a different orbit. All these orbits respect an integral I_2 in addition to the energy because each orbit is confined to a curve.

There are two types of closed curve in Figure 3.9, corresponding to the two basic types of orbit that we have identified. The lower panel of Figure 3.8 shows the spatial form of the loop orbit that generates the curve marked 1 in Figure 3.9. At a given energy there is a whole family of such orbits that differ in the width of the elliptical annuli within which they are confined—see Figure 3.10. The unique orbit of this family that circulates in